



Influence of a thin amorphous surface layer on de-channeling during aluminum implantation at different temperatures into 4H-SiC

M. K. Linnarsson¹ · A. Hallén² · L. Vines³

Received: 4 June 2019 / Accepted: 7 November 2019 / Published online: 19 November 2019
© The Author(s) 2019

Abstract

Ion implantation is an important technique in semiconductor processing and has become a key technology for 4H-SiC devices. Today, aluminum (Al) implantations are routinely used for p-type contacts, p⁺-emitters, terminations and many other applications. However, in all crystalline materials, quite a few ions find a path along a crystal channel, so-called channeling, and these ions travel deep into the crystal. This paper reports on the channeling phenomenon during Al implantation into 4H-SiC, and in particular, the influence of a thin native oxide will be discussed in detail. The effects of thermal lattice vibrations for implantations performed at elevated temperatures will also be elucidated. 100 keV Al ions have been implanted along the [000-1] direction employing samples with 4° miscut. Before implantation, the samples have been aligned using the blocking pattern of backscattered protons. Secondary ion mass spectrometry has been used to record the Al depth distribution. To predict implantation profiles and improve understanding of the role of crystal structure, simulations were performed using the Monte-Carlo binary collision approximation code SIIMPL. Our results show that a thin surface layer of native oxide, less than 1 nm, has a decisive role for de-channeling of aligned implantations. Further, as expected, for implantations at elevated temperatures, a larger degree of de-channeling from major axes is present due to increased thermal vibrations and the penetration depth of channeled aluminum ions is reduced. The values for the mean-square atomic displacements at elevated temperatures have been extracted from experimental depth profiles in combination with simulations.

1 Introduction

Ion implantation is an important technique in device manufacturing, in particular for silicon carbide (SiC), since diffusion of dopants is negligible at typical process temperatures [1, 2]. For most of the technologically used doses, SiC will become damaged and the lattice structure will be hard to

restore if the implantation is performed at room temperature (RT). Therefore, ion implantations in SiC are usually performed at elevated temperature to preserve the crystallinity. In addition, high-temperature post-implantation annealing (above 1600 °C) is needed to recover the lattice and reach high dopant activation. Due to the negligible diffusivity of most dopants, these high-temperature activations do not significantly change the implantation profiles.

Typically, ion implantation is performed in some “random,” non-channeling direction to minimize channeling effects. The standard miscut, 4° off-axis from the [0001] toward the [11–20] direction, of SiC wafers is commonly used as a non-channeling direction for implantation into 4H-SiC. This results in a more or less Gaussian dopant depth distribution, where the depth is determined by the used ion energy and the target stopping power. However, a substantial amount of ions usually finds a crystal channel [3, 4], which results in a profile that extends considerably deeper than predicted and this may influence, for instance, the position of an electrical pn junction. On the other hand, if ion implantation is performed along, or close to, a major crystal direction, the channeled ions interact less with the target

✉ M. K. Linnarsson
marga@kth.se

A. Hallén
ahallen@kth.se

L. Vines
lasse.vines@fys.uio.no

¹ Materials and Nano-Physics, Department of Applied Physics, School of SCI, KTH Royal Institute of Technology, Electrum 229, 164 40 Kista, Sweden

² Department of Electronics, School of EECS, KTH Royal Institute of Technology, Electrum 229, 164 40 Kista, Sweden

³ Physics Department/Center for Materials Science and Nanotechnology, University of Oslo, Blindern, P.O. Box 1048, 0316 Oslo, Norway

atoms, and therefore, the channeled ions may penetrate up to several times the projected range of the corresponding random implant in 4H-SiC [3, 5–8]. In 4H-SiC device design, several attempts have been made to take advantage of the channeling phenomena to create deep, box-shaped profiles [9, 10]. However, most dopant implantations in SiC are performed at elevated temperature to suppress damage formation and hence thermal vibrations increase and less deep channeling profiles are expected at elevated temperatures. In addition to nuclear and electronic stopping, the extension of a channeled implantation profile is limited by the presence of a thin surface top layer consisting of adhesive contaminants and natural oxide. For example, in normal air ambient, a native oxide, 1 nm thick, is rapidly formed on SiC [11].

To support and explain experimental results, Lindhard developed in the 1960s a theoretical description of channeling where he introduced the concept of “critical angle for channeling” [12, 13]. In this model, the probability for channeling is expressed as the maximum angle between the incoming beam and the axial row of atoms for which the ions still will be steered along the axis. The model is quite simple, based on atomic number, energy of impacting ions and atomic distances in the crystal, but the model has been very useful to predict experimental results for many semiconductors [14, 15]. For more detail, three-dimensional Monte-Carlo simulation codes have been developed for SiC using the binary collision approximation (MC-BCA) [16–20]. These codes originate from the algorithms described and implemented by Robinson et al. in the so-called MARLOWE code [21]. Unfortunately, the MC treatment is more time consuming compared to the straight forward concept of critical angle for channeling.

The increasing importance of SiC devices motivates us to take a closer look at channeling phenomena for Al implantations in 4H-SiC. In this study, two important aspects of channeling will be discussed: first, the effect from a thin amorphous, non-aligned, surface region and second, the influence from thermal vibrations during implantations at elevated temperatures. 100 keV Al⁺ ions have been employed for the implantation at temperatures between RT and 600 °C. The ion beam has been aligned in parallel to the 4H-SiC(0001) direction, and Monte-Carlo simulations using the binary collision approximation have been utilized to support the experimental results. 3D simulations have been employed to illustrate the expected distribution of channeled and de-channeled ions. It is shown that in addition to the used implantation temperature, the thin amorphous surface layer has a strong effect on the depth profiles.

2 Experimental

A 4H-SiC wafer with a low doped, 5×10^{15} N/cm³, 10 μm epitaxial layer has been employed and samples of 5 × 11 mm² size have been cut from the wafer. Before implantation, the sample was aligned and the ion beam struck the sample along the [000-1] direction. The error involved in the alignment of the crystal together with the beam divergence is $\leq 0.1^\circ$. For the sample alignment, 100 keV protons were employed and a six-axis, high-precision goniometer was used. The blocking pattern for the backscattered protons was recorded with an area sensitive, 120-mm-diameter detector. After alignment, the source was reconfigured to produce Al ions.

Single-energy implants with 100 keV Al ions and doses between 2.5×10^{12} and 2.5×10^{14} cm⁻² have been performed in different areas of the same sample. Typically, an area of 1.5 × 1.5 mm² was implanted and a low-dose rate was employed. Both room temperature (RT) and elevated temperatures have been used, i.e., the RT implantation was followed by (in situ) implantations at 600, 400 and 200 °C in different areas of the same sample.

The Al depth distribution in the 4H-SiC samples were determined by secondary ion mass spectrometry (SIMS) using a Cameca ims7f instrument. A primary sputtering beam of 10 keV ³²(O₂)⁺ ions was applied and secondary ²⁷Al⁺ ions were detected. The primary beam was rastered over an area of 200 × 200 μm² and the ion signal was recorded from the central part of this area (~ 60 μm in diameter) after which the crater depths were measured by a Dektak 8 stylus profilometer. A constant erosion rate was assumed for the conversion from sputter time versus depth. The exact implanted doses of the samples used in this study were determined by integrating the recorded SIMS profiles. For conversion of counts to concentrations in the recorded SIMS profiles, a 4H-SiC reference sample implanted with 120 keV Al ions to a dose of 5×10^{14} cm⁻² has been employed.

3 Simulation

To improve the understanding of Al implantation profiles, experimental data have been combined with simulations using the Monte-Carlo binary collision approximation (MC-BCA) code SIIMPL [20]. The simulation code uses the universal potential of Ziegler, Biersack and Littmark (ZBL) [22], and scattering integrals are solved by the “Magic-Formula” [23]. In order to describe the lower electronic stopping in channels, the random electronic loss, S_e , is modified and given by,

$$\Delta E = S_e A \exp(-sp/a_u), \quad (1)$$

where S_e is expressed as kE^b in the used range ($< E_F$, the Fermi energy) and the constants k and b are taken as 4.0 and 0.52, respectively [24]. The electronic stopping is normalized by the constant A , p is the impact parameter and a_u is the universal screening length corrected by a factor s . To estimate the number of displaced atoms, the model suggested by Kinching Pease [25] has been used. Displacement energies of 20 and 35 eV have been utilized for C and Si atoms, respectively [26]. At elevated temperatures, increased dynamic annealing of damage has been accounted for [20]. Thermal vibrations have been included in the model according to the mean-square displacement of matrix atoms where values at RT are from reference 27, while at elevated temperatures, mean-square displacements have been determined from fitting of implantations with different doses. The non-aligned, top layer is represented by an amorphous SiC layer in the simulations. In the SIIMPL code, for an amorphous target, the position of the next collision partner is randomly chosen in a cylinder in front of the ion and the type of ion is randomly chosen among the atoms defined in the unit cell, weighted by their relative abundance [20]. The density of amorphous SiC has been used in the simulations.

4 Results and discussion

Figure 1 shows a blocking pattern of backscattered protons from a 4H-SiC sample. This kind of measurement has been utilized for sample alignment as the blocking pattern provides a map of planar and axial channels. The intensity is given by colors where dark blue stands for lower concentration of backscattering and represents high-symmetry axis

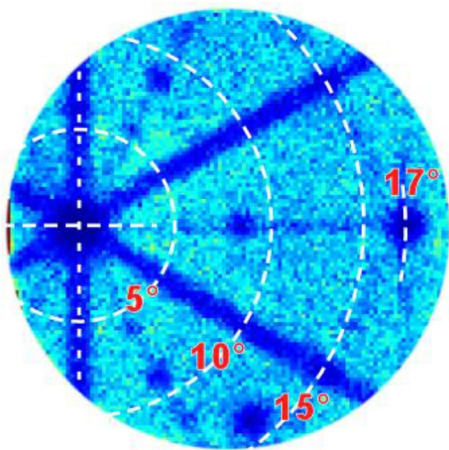


Fig. 1 Blocking pattern for 4H-SiC probed with 100 keV protons. Backscattered angles of 5°, 10°, 15° and 17° from 0°, the [0001] direction, are included in the polar map as white dotted lines

and planes. The six-fold symmetry of 4H-SiC is seen from the {11-20} planes intersecting other {11-20} planes along the [0001] direction. The off angles of 5°, 10°, 15° and 17° from the [0001] direction, used as the 0° direction, in the polar map are indicated by white dotted lines. To the right, 17° from [0001], in the {1-100} plane, a large crystal channel, the $<11-23>$ direction, is clearly visible as a dark spot. For Al ions, a slightly larger critical angle for channeling is expected than for the protons used to collect the blocking pattern. This is due to a larger atomic number and lower velocity for Al ions compared to protons of the same energy [3, 5, 13]. As seen in Fig. 1, a large amount of possible channeling directions are available and after a few collisions, relatively independent of the impact angle, some ions will be guided into low index directions and planes of the crystal and these ions may be found deep into the crystal and also more laterally distributed than the original impact direction.

The 4H-SiC samples have been aligned and the Al implantations have been performed at RT along the [000-1] crystal direction. In Fig. 2, experimental Al depth profiles are shown for three implantations performed with doses 2.8×10^{12} (low), 2.5×10^{13} (medium) and 2.5×10^{14} (high) cm^{-2} , respectively. A logarithmic scale has been used for the concentration in Fig. 2. The lowest used dose is below the point where damage starts to accumulate in the channels and limit the ion paths. For this dose, the depth profile is box shaped with a small peak at 0.11 μm . As the dose increases,

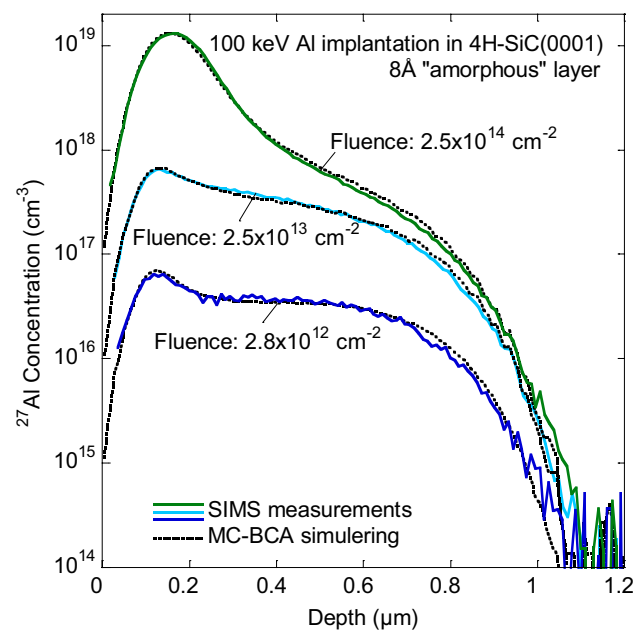


Fig. 2 SIMS measurements and MC-BCA simulation with the code SIIMPL of three Al implantations into 4H-SiC parallel to the [0001] direction. 100 keV Al^+ ions and doses 2.8×10^{12} , 2.5×10^{13} and 2.5×10^{14} cm^{-2} have been used. In the simulations, the native oxide is represented by an amorphous 8 Å thick top layer

the crystal channels will contain an increasing number of displaced C and Si atoms, and therefore, the probability for de-channeling of Al ions increases, and a small decrease in Al concentration with depth is observed for the medium dose. At the highest dose, a large number of interstitial atoms have blocked the channels and an Al peak starts to build-up similarly as in a random target. In addition to experimental SIMS results, MC-BCA simulations using the SIIMPL code have been included in Fig. 2. Fitting parameters used in these simulations will be discussed in the following text.

To further investigate the origin of the small peak observed at 0.11 μm for the low- and medium-dose samples in Fig. 2, the effect from a thin, non-aligned top layer of various thicknesses on “de-channeling” is investigated by MC-BCA simulations. Figure 3 illustrates this “de-channeling” effect of Al ions when passing through a thin amorphous SiC top layer, which is present on the single crystalline 4H-SiC (0001) samples. The Al concentration is displayed versus depth for four different thicknesses, 0, 4, 8 and 16 \AA of the amorphous surface layer, where the depth scale includes the surface layer thickness. In addition to simulations, experimental data has been included in Fig. 3. To avoid build-up of damage, the low-dose case (Fig. 2), $2.8 \times 10^{12} \text{ cm}^{-2}$, has been used in the MC-BCA simulations. As the thickness of the amorphous layer increases, the scattering in the non-aligned surface layer increases and the peak around 0.11 μm increases in height. This depth corresponds to the projected

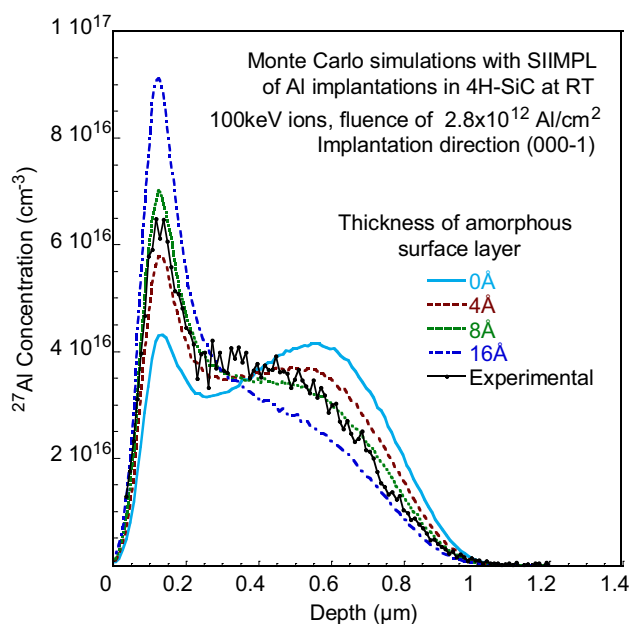


Fig. 3 MC-BCA simulation of Al implantations into 4H-SiC, where the ions are entering along the [000-1] direction. An amorphous SiC surface top layer with a thickness of 0, 4, 8 or 16 \AA has been assumed in the simulation using the SIIMPL code [20]. In addition, experimental data have been included

range for implantations made in a non-channeling (random) direction according to the SRIM2013 code [22, 27]. In addition, the shape of the Al profile at depths between 0.3 and 1.1 μm also changes and the concentration decreases faster with depth, as the amorphous layer thickness and the de-channeling of Al ions increase. Hence, in order to reproduce the experimental data between 0 and 0.2 μm , a scattering top layer has to be included in the simulations. If the native oxide of 4H-SiC in Fig. 2 is represented by an 8 \AA thick amorphous layer, an excellent agreement between MC-BCA simulations and experimental data is obtained. This thickness corresponds well with the literature values of 9.3 \AA , measured by angle-resolved x-ray reflectivity, for a native oxide that consists mainly of silicon oxycarbide species after exposures of SiC to air [11]. The small discrepancy can be explained with a slightly lower density of the silicon oxycarbide layer compared to amorphous SiC utilized in the simulation.

For device applications, ion implantations are commonly performed at elevated temperatures to reduce the ion-induced damage and maintain the crystal structure. This will have a strong influence on channeled profiles, as previously discussed. In Fig. 4, implantations performed at RT as well as 200, 400 and 600 $^{\circ}\text{C}$ are shown. The low-dose cases have been used to eliminate contribution from damage build-up and annealing. In the displayed depth profiles, a linear concentration scale has been used. As the temperature increases, the thermal vibrations increase and result in a larger probability for de-channeling and, therefore, less deep profiles. The effect from the upper most non-aligned layers is less visible as the temperature increases and it cannot be separated from the increasing contribution from de-channeling due to increasing lattice vibrations in the 600 $^{\circ}\text{C}$ depth profile. In the SIIMPL code, the thermal vibrations have been included at RT, as the mean-square displacement for carbon and silicon atoms, 0.051 and 0.057 \AA , respectively, according to x-ray diffraction measurements in 6H-SiC [28]. The simplifying assumption taking the average of lattice vibrations over the crystal, independent of crystal directions, is used and any possible difference between 4H-SiC and 6H-SiC has been neglected. At elevated temperatures, the mean-square displacement values are determined from fitting of implantation depth distribution with different doses and temperatures. The values used are listed in Table 1. Note that a larger displacement is expected for carbon compared to silicon due to a lower mass. No detailed investigation has been made to separate the contribution from carbon and silicon vibrations and as a first approximation, the relative contribution from carbon and silicon has been scaled according to the relative mean-square displacement at RT for carbon and silicon. However, this ratio may decrease at elevated temperature as theoretical calculations suggest that the values of the mean-square displacement for carbon and silicon approach each

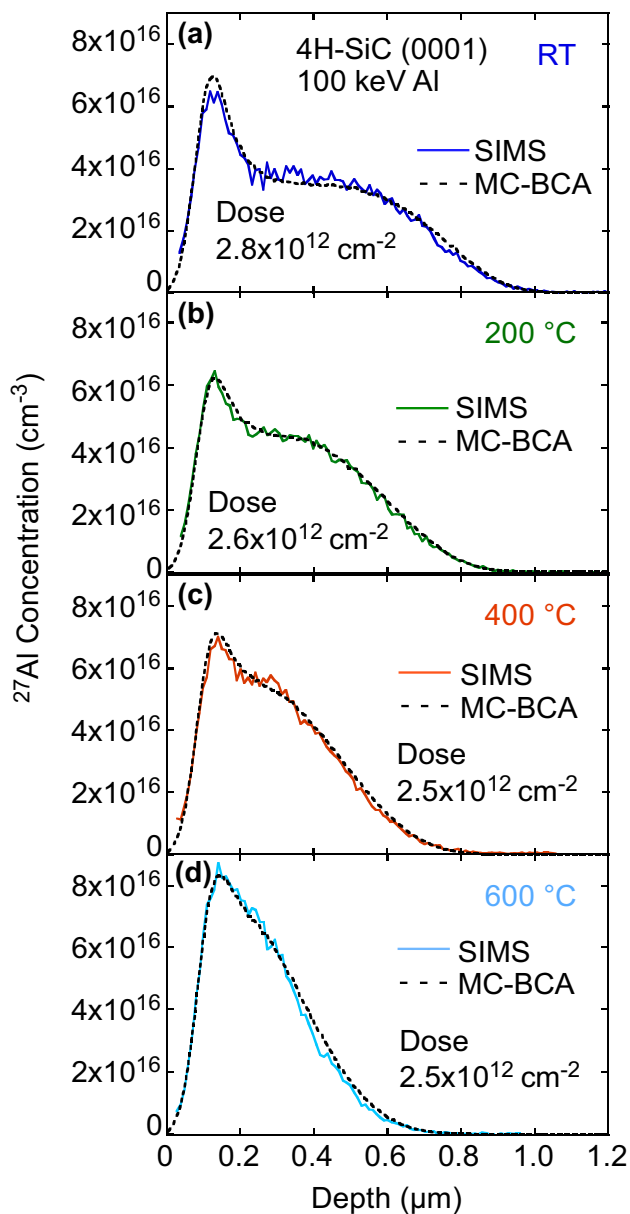


Fig. 4 Al concentration versus depth in four 4H-SiC samples implanted at RT (a), 200 °C (b), 400 °C (c) and 600 °C (d). 100 keV Al ions have been implanted along the [000-1] crystal direction. The SIMS data are drawn as solid lines while MC-BCA simulations are drawn as dotted lines

Table 1 Mean-square displacement for carbon and silicon atoms used in the SIIMPL code

Temperature	Mean-square displacement	
	Carbon atoms	Silicon atoms
RT	0.057 Å	0.051 Å
200 °C	0.070	0.063
400 °C	0.080	0.072
600 °C	0.091	0.082

other at high temperatures [28]. In this context, it should be pointed out that identical simulation curves can be obtained using the same mean-square displacement for both carbon and silicon. For example, at 400 °C, using 0.074 Å as the mean-square displacement for carbon and silicon gives the same simulation result for channeling along the [000-1] direction as the numbers 0.080 and 0.072 Å for the mean-square displacement of carbon and silicon, respectively.

To better describe the native oxide at elevated temperatures, a 4 Å thick, amorphous SiC top layer has been assumed in the MC-BCA simulations. Such a reduction in the layer thickness at 200, 400 and 600 °C is motivated by desorption of surface contaminants during the treatment at 600 °C and it may also improve the lattice match of the native oxide. As seen from Fig. 4, the experimental data at different temperatures are perfectly reproduced in the simulations including the mentioned approximations of the mean-square displacement.

3D simulations have also been performed to trace the ion paths in detail and to include the contribution from de-channeling at elevated temperatures. Figure 5 displays 2D images sliced out from 3D simulations of Al implantations performed at temperatures between RT and 600 °C with doses according to the experimental data in Fig. 4. Figure 5 includes top views where the final position of all tracked ions is monitored as black dots and cross sections, i.e., thin slices of the {1-100} plane, where the color gives the “intensity,” or the probability, to find an ion at a particular position. The sample has been aligned and the incoming beam is along the [000-1] direction. In the simulations 5×10^6 ions have been tracked and a small impact area of 1 nm², in which each ion position is randomly selected, has been used in the simulations. Such a small area is used to highlight preferential crystal directions and degree of de-channeling and to avoid overlapping and averaging of the output. Here it should be pointed out that if implantation is made with such a low dose in a device, as in Fig. 4, less than one ion will on average hit this small area and the simulation displays probability to find Al ions in a particular position. The intensity is displayed in colors utilizing a linear scale, where the highest probability is given in red and blue represents the lowest intensity. Different intensity scales have been used at different temperatures to easily find the depth for the maximum probability. Starting at the surface with an impact area of 1 nm², at the depth of 0.11 μm (the projected range in a random target), the lateral spread of ions is much larger and the probability to find an ion 0.1 μm laterally from the original direction is high. For all temperatures up to and around the projected range, the distributions are similar. Below the random projected range, most of the ions follow the [000-1] channel but there is a blue, cone-shaped envelope of de-channeled ions. At RT, quite a few ions reach a depth of 1.1 μm and the highest probability to find an ion in the original channel direction

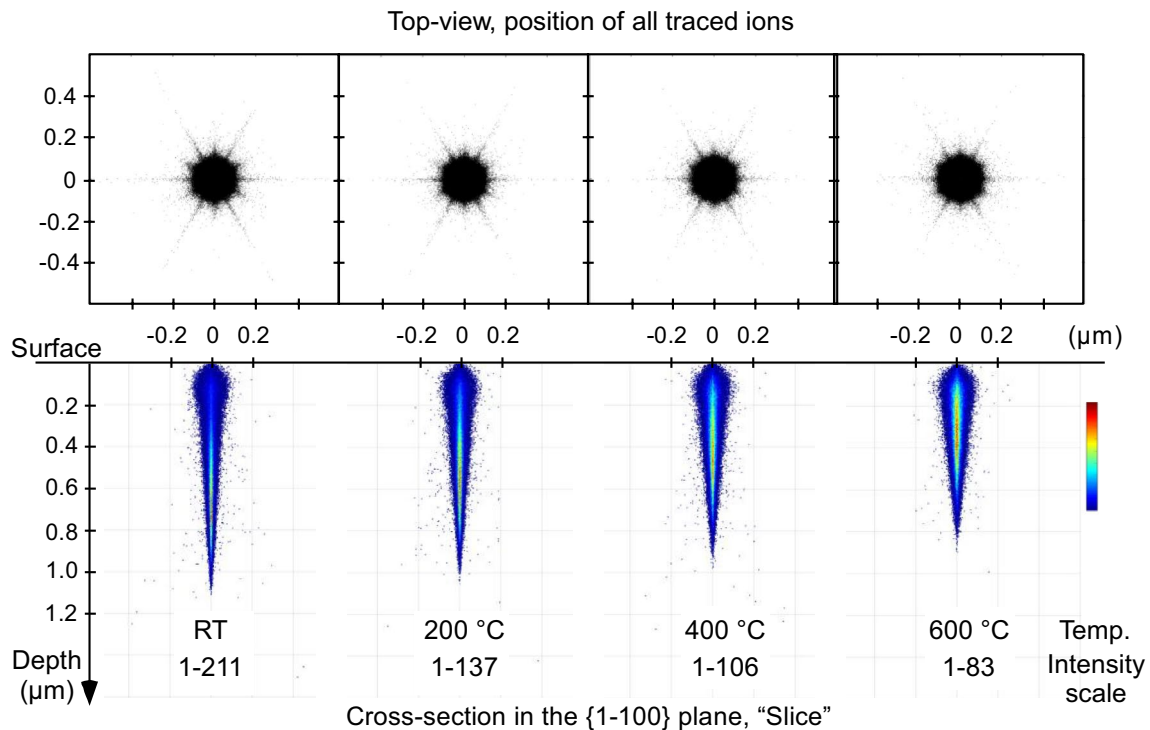


Fig. 5 3D simulation of implantation of 100 keV $^{27}\text{Al}^+$ ions along the [000-1] direction in 4H-SiC at RT and 200, 400 and 600 °C. In the simulations, an impact area of $1 \times 1 \text{ nm}^2$ has been used. On top, a total amount of ^{27}Al ions from the whole volume shown in black and below the cross section, represented by a slice in the {1-100} plane,

is displayed. The colors are used for the intensity scale. Different scales are used for different temperatures due to a higher confinement to the [000-1] channel at RT compared to implantations at elevated temperatures

is around 0.7 μm (red color). Note also that the ions are more confined to the crystal direction at RT compared to implantation performed at elevated temperatures. As the temperature increases, the channeling depth is reduced and the probability for de-channeling increases. The "cone" around the channel direction has a broader base and shorter length. The highest probability of well-channeled ions along the main track moves closer to the surface, and at 600 °C, the maximum is found around 0.5 μm. Taking a closer look shows that there is also a small probability, a few blue dots, to find Al ions distributed far out laterally from the main channel. This is supported by the top view, where the six-fold symmetry of the lattice is revealed with an increased probability for the ions in the {1-100} and {11-20} planes. In the {1-100} plane, the main contribution is from $\langle 11-23 \rangle$ crystal directions, 17° off from the original beam direction. In addition, a few ions are found far away from the central track.

In conclusion, if channeling implants will become a useful tool for deep box implantations in devices, at least three basic aspects have to be concerned. These are i) surface oxides, ii) implantation temperature and iii) high probability for ions to be steered into various crystal directions and planes. However, by MC calculations, the contribution of these three effects can be predicted.

5 Summary

The native oxide of 4H-SiC plays a decisive role for de-channeling of aligned implantations of Al along the [000-1] direction. At RT, an 8 Å thick amorphous layer is needed in the simulations to fit the experimental results, which is a thickness in agreement with what is expected from the native oxide. Furthermore, a decrease in thickness of the scattering non-aligned top layer from 8 to 4 Å is revealed for samples heat treated at 600 °C and sequentially implanted at 200, 400 and 600 °C, indicating a desorption from the top layer (baking).

As the implantation temperature increases, the thermal vibrations increase and result in larger de-channeling and shallower profiles. The effect of the uppermost non-aligned layers becomes less visible after implantation at elevated temperatures. At 600 °C, the contribution to de-channeling from the non-aligned top layer cannot be separated from the increasing de-channeling caused by increasing thermal vibrations of carbon and silicon atoms. According to simulations and experimental data, as the temperature is increased from RT to 600 °C, the mean-square displacement is increased with 60% and, accordingly, the channeling depth is reduced.

Acknowledgements Open access funding provided by Royal Institute of Technology. Financial support by the Swedish Research Council (VR E0510501), the Ion Technology Centre, ITC, in Sweden via VR-RFI (contracts #821-2012-5144 and #2017-00646_9) and the Swedish Foundation for Strategic Research (SSF, contract RIF14-0053) and the Research Council of Norway through the research project FUNDA-MeNT (no. 251131) and the Norwegian Micro and Nano-Fabrication Facility NorFab (no. 245963) are gratefully acknowledged.

Open Access This article is distributed under the terms of the Creative Commons Attribution 4.0 International License (<http://creativecommons.org/licenses/by/4.0/>), which permits unrestricted use, distribution, and reproduction in any medium, provided you give appropriate credit to the original author(s) and the source, provide a link to the Creative Commons license, and indicate if changes were made.

References

1. T. Kimoto, K. Kawahara, H. Niwa, N. Kaji, J. Suda, International Workshop on Junction Technology (IWJT). IEEE Proc. **2014**, 1 (2014)
2. A. Hallén, M.K. Linnarsson, Surf. Coat. Tech. **306**, 190 (2016)
3. D.S. Gemmell, Rev. Mod. Phys. **46**, 129 (1974)
4. K. Nordlund, F. Djurabekova, G. Hobler, Phys. Rev. B **94**, 214109 (2016)
5. A. Vantomme, Nucl. Instr. Meth. B **371**, 12 (2016)
6. J. Wong-Leung, M.S. Janson, B.G. Svensson, J. Appl. Phys. **93**, 8914 (2003)
7. A. Hallén, M.K. Linnarsson, L. Vines, Mat. Sci. Forum **963**, 375 (2019)
8. M.K. Linnarsson, A. Hallén, L. Vines, B.G. Svensson, Mat. Sci. Forum **963**, 382 (2019)
9. US Patent Application Publication US 2015/0028350 A1, Jan. 29, 2015, Cree Inc.
10. US Patent Application Publication US 2018/0069083 A1, Mar. 8, 2018, Cree Inc.
11. C. Önnby, C.G. Pantano, J. Vac. Sci. Technol. **A15**, 1597 (1997)
12. J. Lindhard, Phys. Lett. **12**, 126 (1964)
13. J. Lindhard, Mat. Fys. Medd. Dan. Vid. Selsk. **34**, 14 (1965)
14. S.T. Picraux, J.A. Davies, L. Eriksson, N.G.E. Johansson, J.W. Mayer, Phys. Rev. **180**, 873 (1969)
15. G. Hobler, Radiat. Eff. Def. Sol. **139**, 21 (1996)
16. M. Posselt, B. Schmidt, T. Feudel, N. Strecker, Mater. Sci. Eng. **B71**, 128 (2000)
17. G. Lulli, E. Albertazzi, M. Bianconi, R. Nipoti, M. Cervera, A. Carnera, C. Celini, J. Appl. Phys. **82**, 5958 (1997)
18. G. Hobler, Nucl. Instr. Meth. **B96**, 155 (1995)
19. E. Morvan, P. Godignon, J. Montserrat, J. Fernández, D. Flores, J. Millán, J.P. Chante, Mat. Sci. Eng. **B46**, 218 (1997)
20. M.S. Janson, PhD Thesis, KTH-Royal Institute of Technology 2003, ISSN0284-0545
21. M.T. Robinson, I.M. Torrens, Phys. Rev. B **9**, 5008 (1974)
22. J.F. Ziegler, J.P. Biersack, Y. Litmark, The stopping and ranges of ions in solids. Pergamon Press, Oxford (1985)
23. J.P. Biersack, L. Haggmark, Nucl. Instr. Meth. **174**, 257 (1980)
24. M.S. Janson, M.K. Linnarsson, A. Hallén, B.G. Svensson, J. Appl. Phys. **96**, 164 (2004)
25. G.H. Kinching, R.S. Pease, Rep. Prog. Phys. **18**, 1 (1955)
26. V. Heera, W. Skorupa, Mat. Res. Symp. Proc. **438**, 241 (1997)
27. Nuclear Energy Agency, data bank, computer service, <https://www.oecd-nea.org/tools/abstract/detail/nea-0919/>
28. A. Zywietz, K. Karch, F. Bechstedt, Phys. Rev. B **54**, 1791 (1996)

Publisher's Note Springer Nature remains neutral with regard to jurisdictional claims in published maps and institutional affiliations.